Solar wind excitation of Pc5 fluctuations in the magnetosphere and on the ground

R. L. Kessel[1]

Received 15 January 2007; revised 24 October 2007; accepted 19 December 2007; published 3 April 2008.

[1] The primary purpose of this paper is to show the importance of solar wind excitation as a source of magnetospheric and ground Pc5 fluctuations. In particular, we show that pressure fluctuations, a nearly ubiquitous feature of the solar wind, drive magnetospheric compressional Pc5, whose amplitude and power increase in direct proportion to the amplitude and power of the solar wind pressure fluctuations. Previous studies of compressional Pc5 have focused primarily on internally generated waves on the dusk flank; here we highlight the pressure fluctuations associated with geoeffective high-speed streams (HSSs) and interplanetary coronal mass ejections (ICMEs) during a time interval in March and April 2002, in the declining phase of the solar cycle, when there was a favorable alignment of satellites. Using three examples and a statistical survey, we show that for this time interval external forcing due to solar wind dynamic pressure fluctuations was dominant over internal forcing. Fluctuations driven by internal processes, occurring primarily at dusk and on the nightside, accounted for less than 20% of the total power. We also found that multiple external forcing processes were occurring during this interval, including evanescent propagation of compressional waves, field line resonance (FLR), and global mode excitation. We need to enlarge our vision of the source of ULF waves to include excitation by solar wind pressure fluctuations as a significant factor.

Citation: Kessel, R. L. (2008), Solar wind excitation of Pc5 fluctuations in the magnetosphere and on the ground, *J. Geophys. Res.*, *113*, A04202, doi:10.1029/2007JA012255.

1. Introduction

[2] Ultra low frequency (ULF) waves have been extensively studied for many years both on the ground and in space. Solar wind sources of magnetospheric ULF waves was the subject of a geophysical monograph in 1994, but the subject is not closed. Transmission scenarios have been postulated from relatively simple (e.g., reconnection) to more complicated (e.g., cavity modes) and in between. We focus here on the lowest frequency ULF waves, the Pc5 frequency range, $\sim$1–8 mHz, and are particularly interested in those driven by the solar wind. Two types of Pc5 waves are commonly found in the magnetosphere, compressional and toroidal [e.g., *Anderson*, 1994]; toroidal waves are solar wind driven at the magnetopause flanks, but compressional waves have typically been linked to internal processes. Compressional Pc5 waves have their largest fluctuation in the direction of the magnetic field but usually also have a comparable transverse component in the radial direction; they can excite the polodial mode. Toroidal Pc5 waves have their largest component in the azimuthal direction. Polodial and toroidal modes represent two limits of the hydromagnetic wave equations [e.g., *Hughes*, 1994] for standing waves on magnetic field lines. Frequently, the two modes are mixed. If the amplitudes are large enough, then the waves can be measured on the ground. However, on the ground the signal includes magnetotelluric effects that must be separated out to isolate those due to solar wind sources [e.g., *Pilipenko and Fedorov*, 1994]. We first review relevant observations and analysis of these waves.

[3] *Anderson* [1994] showed toroidal Pc5 waves to be mainly on the dawn flank, stronger at higher L shells. The most frequently cited source of these flank Pc5 pulsations is the Kelvin-Helmholtz (K-H) instability at the magnetopause [e.g., *Dungey*, 1955; *Miura*, 1992; *Anderson*, 1994]. Fast magnetosheath flow excites surface waves on the magnetopause that become Kelvin-Helmholtz unstable [e.g., *Miura*, 1984]. The amplitude of the surface waves decays evanescently into the magnetosphere causing them to be weaker on lower *L* shells. *Mann et al.* [1999] have recently shown that for very large flow speeds at the magnetopause flanks, the K-H instability can energize body type waveguide modes. The waveguide model is similar to the cavity model except that the cavity remains open downtail; waveguide modes propagate antisunward at the natural frequencies of the magnetosphere [e.g., *Harrold and Samson*, 1992; *Mann et al.*, 1999]. Others have proposed that upstream shock-related pressure oscillations could drive magnetopause surface waves with periods in the Pc5 range [e.g., *Sibeck et al.*, 1989; *Fairfield et al.*, 1990; *Fairfield et al.*, 2003]. *Engebretson et al.* [1998, and references therein] suggested both direct driving and K-H instability might play a role, i.e., the solar wind could provide a source of Pc5

[1]NASA Goddard Space Flight Center, Greenbelt, Maryland, USA.

This paper is not subject to U.S. copyright.
Published in 2008 by the American Geophysical Union.

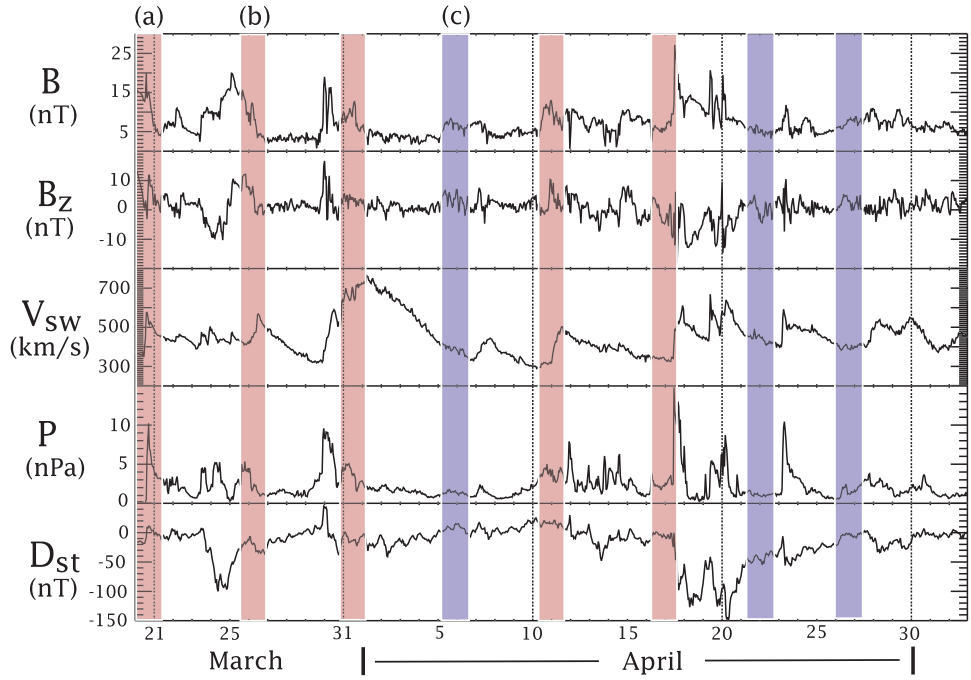

Figure 1. Solar wind parameters from OMNI during the interval 20 March to 2 May 2002. From top to bottom are shown magnetic field magnitude; B_z; flow Speed, flow Pressure, and D_{st}.

wave energy to the magnetosphere or solar wind waves could act as seed perturbations to drive boundary displacements that are amplified by the K-H instability. *Zhu and Kivelson* [1991] found transverse waves polarized in the azimuthal direction (toroidal) on the nightside at higher latitude. *Zhu and Kivelson* [1991] associated their nightside, high-latitude toroidal waves with substorms.

[4] The study of compressional Pc5 waves and fluctuations has focused on the magnetopause flanks, especially the nightside dusk flank. *Anderson*'s [1994] review of ULF pulsations found that the primary occurrence region of compressional Pc5 was on the dusk flank at large L (his Figure 1). The waves were more likely on the nightside and also occurred on the nightside dawn flank. *Zhu and Kivelson* [1991] using ISEE-1/2 found that compressional Pc5 waves were a common feature near the two flanks of the magnetosphere, polarized in a meridian plane with comparable compressional and transverse amplitudes. The waves have larger amplitude at magnetic latitudes below 20° than at higher latitudes and are largest at the magnetopause, decreasing in power with lower L shell. *Barfield and McPherron* [1972], in a study at geostationary orbit, found compressional waves on the nightside dusk flank that were linearly polarized in a meridian plane with nearly equal compressional and transverse components (possibly polodial). Barfield and McPherron attributed compressional Pc5 waves on the nightside dusk flank to substorm enhancement of the partial ring current. They found that the waves occurred at the local time of the maximum development of the partial ring current, at or shortly after the onset of a substorm. *Anderson* [1994] advocated that compressional Pc5 pulsations on the nightside flanks were due to local wave particle interactions.

[5] *Zhu and Kivelson* [1991] also found compressional Pc5 waves on the dayside but their coverage of this area was not as complete as in other regions. They attributed these waves to solar wind dynamic pressure variations. *Kepko et al.* [2002] showed pressure fluctuations at the same discrete frequencies in the solar wind as compressional waves at geostationary orbit. Recent GOES observations [*Kessel et al.*, 2003] showed sustained geomagnetic pulsations in the noon and midnight sectors during times of sustained dynamic pressure fluctuations in the solar wind.

[6] Across the dayside magnetopause the simplest transmission mechanism is direct entry of waves when the magnetopause is a rotational discontinuity, $B_n \neq 0$. Satellite observations have shown that the magnetopause can stably exist as either a tangential or rotational discontinuity [e.g., *Russell and Elphic*, 1978; *Sonnerup et al.*, 1981]. *Kwok and Lee* [1984] determined theoretically that MHD wave transmissions can occur over a wide range of incident angle for RDs and that the transmitted waves were usually amplified. They suggested that MHD wave transmission at an open magnetopause can be a significant mechanism for energy transport from the magnetosheath to the magnetosphere.

[7] *Wright and Rickard* [1995] showed that broadband fluctuation power in the solar wind can lead to enhanced excitation of the magnetospheric cavity or waveguide modes if the spectrum of driving fluctuations includes the cavity eignfrequencies. Large-scale structures such as rotational and tangential discontinuities, current sheets, magnetic holes and clouds, and high-speed streams [e.g., *Burlaga*, 1968; *Lepping and Behannon*, 1986; *Kessel and Chen*, 1999], or small-scale structures, inhomogeneities, or perturbations impact the Earth's magnetosphere and excite various modes of oscillation. The spectrum includes waves in the frequency range 0.001 mHz to 1 Hz. *Kivelson et al.* [1984] proposed that the magnetospheric cavity as a whole can ring as a result of solar wind excitation and have its own

set of cavity eigenperiods. The Earth's magnetospheric cavity extends from an outer boundary, possibly the magnetopause (or bow shock), to an internal turning point possibly near the plasmapause. In the cavity model energy is input into the magnetosphere and the cavity as a whole rings at its own eigenfrequenices.

[8] Assuming waves have been excited in Earth's magnetosphere by one of the processes above, at some L shell the period of the Kelvin-Helmholtz surface wave, or the compressional wave, or the cavity eigenperiod will match the period of the local field line and couple, transferring energy from the wave into a field line resonance [*Southwood*, 1974; *Chen and Hasegawa*, 1974; *Hughes*, 1994]. *Dungey* [1954] originally proposed that the regular periods of geomagnetic pulsations might be due to standing Alfvén waves excited on geomagnetic field lines, later termed field line resonances (FLRs). Field line resonances are observed in the Pc5 range with discrete frequencies at approximately 1.3, 1.9, 2.6, and 3.4 mHz [*Ruohoniemi et al.*, 1991; *Samson et al.*, 1992; *Samson and Rankin*, 1994]. *Samson et al.* [1992] showed that these discrete frequencies in the Pc5 frequency range were compatible with MHD waveguide and cavity modes in the magnetosphere. The FLRs are observed on the ground at stations near the magnetic footpoints of the particular field lines that are resonating.

[9] *Kivelson and Southwood* [1991] proposed that pressure perturbations at the magnetopause could cause vortex motions in the ionosphere at footpoints of field lines connected to the magnetopause; the FLR was excited at the magnetopause field lines. *Engebretson et al.* [1991] advocated that the currents (or precipitating electrons) are carried into the cusp as region 1 currents where they cause ac variations in ionospheric Pedersen currents. These in turn set up region 2 currents that propagate to lower latitudes. In this model, where the ionosphere acts like a transitor modulating the flow of current, the energy flow is from the magnetopause into the cusp and then to lower latitudes. *Rae et al.* [2005] recently showed enhanced power at Polar inside the magnetopause and also in the ionosphere with Super Darn. They showed large oscillating Poynting flux in the y and z directions, due to standing Alfvén waves, and suggested that magnetopause oscillations couple energy to field lines close to Polar that also resonate in the ionosphere.

[10] In this paper we used the S3C Great Observatory: specifically, ACE and Wind in the solar wind, Geotail near the magnetopause, GOES 8 and 10 at geostationary orbit, Cluster over the poles, and CANOPUS/CARISMA ground stations near the footpoints of magnetic field lines connected to either the magnetopause or the GOES satellites. In the next section we briefly describe the data we use, the orbits of the satellites and the location of the ground stations with respect to them. We also briefly describe our spectral analysis. Following that we show observations for three intervals: one ICME, one HSS, and one interval with nominal solar wind conditions for comparison. We next show a determination of Poynting flux for one interval and discuss the implications of this for transfer of energy. We then describe a statistical survey from the entire interval, 20 March 2002 through 2 May 2002 and the solar wind dependencies found. We discuss our results and their significance and relationship to prior work. Finally, we list our conclusions.

2. Orbits, Instruments, and Methods

[11] For this study we used data from the ACE, Wind, Geotail, Cluster, and GOES 8 and 10 satellites, along with the CARISMA (formerly CANOPUS) ground-based stations RANK, CONT, DAWS, FSIM, FSMI, and GILL. We focus on the time interval from 20 March to 1 May 2002, during which there were several interplanetary CMEs and high-speed solar wind streams. ACE was 225 R_E upstream near the Sun-Earth line for the entire interval. Wind was upstream between 20 and 80 R_E, but its orbit took it from 100 R_E on the dawnside to 200 R_E on the duskside. For about 1 d of its 5 d orbit, Geotail was skimming the magnetopause on the dayside, crossing between the magnetosphere, boundary layer, and magnetosheath. Cluster data is only available for a few hours each orbit in 2002; during the four intervals studied here data is available for short segments with Cluster either over the northern or southern pole or in the solar wind. GOES 8 and GOES 10 were at geostationary orbit, with GOES 8 about 4 h ahead of GOES 10 in local time.

[12] During March and April 2002, while skimming the dayside magnetopause, Geotail's northern footpoint is near several CARISMA ground stations: RANK, CONT, and DAWS. Geotail's southern footpoint is nearest to MCM ground station on Antarctica. GOES 8's northern footpoint is nearest to GILL, and southern footpoint is nearest SPS. GOES 10's northern footpoint is between FSMI and FSIM, and southern footpoint is nearest MCM. Footpoint traces were found using the SSCWeb interface. Cluster is either over the northern or southern pole or in the solar wind during these four intervals. Footpoint traces for Cluster were also created at the University of Leicester (UK).

[13] All satellite data was obtained from CDAWeb. On ACE, we used magnetic field data from the Magnetic Field Instrument (MFI) and plasma data from the Solar Wind Electron Proton Alpha Monitor (SWEPAM). We used data from the Magnetic Field Investigation (MFI) [*Lepping et al.*, 1995] and the Solar Wind Experiment (SWE) [*Ogilvie et al.*, 1995] on Wind. We used magnetometer data from the Magnetic Field Measurement (MGF) [*Kokubun et al.*, 1994], Comprehensive Plasma Instrument (CPI) [*Frank et al.*, 1992], and the Electric Field Detector (EFD) (1992) instrument on Geotail. We used the FGM data on Cluster [*Balogh et al.*, 2001]. We used the magnetic field instrument on both GOES 8 and GOES 10 [*Singer et al.*, 1996]. CARISMA data was supplied through http://bluebird.phys.ualberta.ca/carisma/carisma.html.

[14] For the solar wind spectral analysis we used both dynamic pressure (nV_{sw}^2) and magnetic field magnitude (compressional waves). Near the magnetopause (Geotail) and in the magnetosphere (GOES) we used magnetic field magnitude (compressional fluctuations) to compare with the solar wind fluctuations. We used 1 min resolution data to provide detail on the Pc5 portion of the spectrum (1–8.3 mHz). Each data set was detrended by subtracting the background field using the IDL smooth function with a window of 61 points (1 h). Other windows from 20 min to 4 h were examined for comparison; the spectral analyses

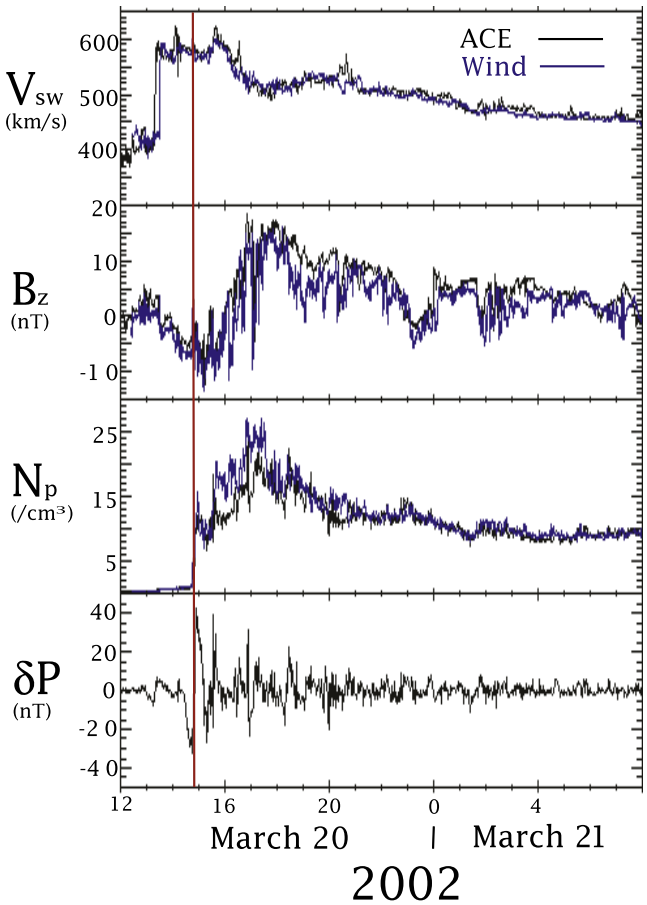

Figure 2. Solar wind parameters for ACE and Wind during interval a.

were not significantly different. The resulting fluctuations were tapered using a Parzen window. The data were processed using a fast Fourier transform algorithm with a sliding 128 point (2 h) window to create power spectral densities (PSD) and then the PSDs were summed from 1 to 8.3 mHz to get total power in the Pc5 range. FFT methods were determined from *Ramirez* [1985] and *Press et al.* [1986].

3. Observations

[15] During March and April 2002, in the declining phase of solar cycle 23 when high-speed streams were prevalent, there was a favorable alignment of satellites that facilitated a study of fluctuations in the Pc5 frequency range, in the solar wind and magnetosphere. Figure 1 shows OMNI data for the interval from 20 March to 2 May when there are more than 10 high-speed solar wind streams, identified by V_{sw} in the middle panel. Near the onset of each stream there is an increase in magnetic field magnitude (top panel) and dynamic pressure (fourth panel). The IMF is primarily northward or near the ecliptic plane during this interval as seen in the B_z component (second panel), with two strong exceptions, one starting on 23 March and the other on 17 April. During these two intervals the magnetosphere reacts with a strong increase in the D_{st} index as seen in the bottom panel. The vertical bars in Figure 1 are aligned with the 1–2 d out of Geotail's approximately 5 d orbit, when Geotail is skimming the flank and dayside magnetopause. Five of these vertical bars are colored red indicating intervals during ICMEs or HSSs and three are colored blue indicating intervals of nominal solar wind speed. We examined all of these intervals in detail and selected three as representative to show here. These are intervals when Geotail's orbit spent a considerable time just inside the magnetopause boundary, i.e., in the magnetosphere versus in the magnetosheath. The selected intervals are marked a–c in Figure 1.

3.1. Interval a

[16] Solar wind parameters for an ICME (magnetic cloud) interval, interval a 20–21 March 2002, are shown in Figure 2 with both ACE and Wind data. Wind data is shown in black and ACE data in blue. ACE is 225 R_E upstream near the Sun-Earth line while Wind is 50 R_E upstream but considerably off the Sun-Earth line, 100 R_E on the dawn side. Solar wind speed is shown in the top panel followed by IMF B_z component (GSE), then solar wind density, and finally dynamic pressure fluctuations. ACE data is shown with a 25 min time delay to compare with Wind IMF and density. As seen in Figure 2 the solar wind speed increase is 10 min out of sync with this time shift. Otherwise, the large-scale features are well aligned at the two satellites which illustrates both the cohesiveness of the structure and the extension over large distances in the y direction. The speed increase (top panel) before the density increase (third panel) and the smooth rotation in IMF direction are typical of ICMEs [e.g., *Zurbuchen and Richardson*, 2006]. The pressure fluctuations are minimal until the density increase at 1445 marked by a vertical line. These fluctuations are a combination of speed and density fluctuations, here the density fluctuations have the larger amplitude.

[17] In Figure 3 we show fluctuations in magnetic field for Geotail, GOES 8 and 10, and Cluster satellites, in the coordinate system used by *Zhu and Kivelson* [1991] described as follows. The z-axis is parallel to the running average magnetic field, **B**, the y-axis is parallel to $\mathbf{r_{pos}} \times \mathbf{z}$ (azimuthal, positive westward), and the x-axis completes the system. In this system b_z is the compressional component. The Polodial mode, radial perturbations in the meridian plane, is identified by b_x and b_z fluctuations. The Torodial mode is identified by (azimuthal) b_y fluctuations. What is immediately obvious comparing Figures 2 and 3 is that geostationary fluctuations (middle six panels) turn on at the time corresponding to the increased solar wind pressure fluctuations impacting Earth's magnetosphere, shown with a solid vertical line (1445 in Figure 2; 1500 in Figure 3). The strongest component in the GOES data for the first 6 h (1500–2100) is the compressional (b_z) component (panels 6 and 9). GOES 8 is on the dayside during this interval passing through the Sun-Earth line at 1700 (dotted vertical line). GOES 10 is 4 h behind GOES 8 and so is on the dawn flank initially and passes through the Sun-Earth line at 2100 (dotted vertical line). Figure 3 shows that the GOES 8 compressional fluctuations on the dayside are higher amplitude than the corresponding compressional fluctuations on the dawnside at GOES 10. We also note the increase in compressional fluctuations at GOES 10 starting about 0200 on 21 April when GOES 10 is on the dusk flank. These

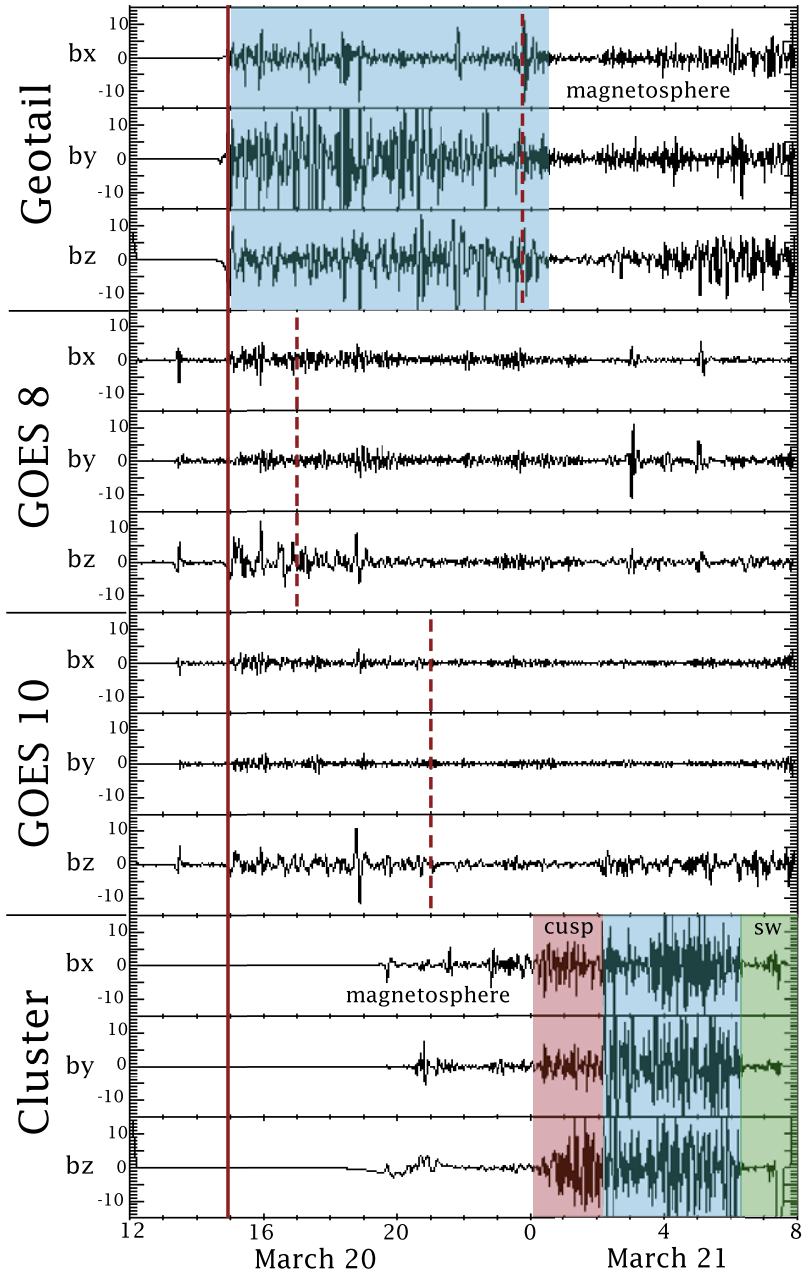

Figure 3. Fluctuations in magnetic field for the Geotail, GOES 8 and 10, and Cluster satellites during interval a.

fluctuations are not directly attributable to solar wind fluctuations. Because the IMF was southward on the leading edge of the ICME, it is likely that these latter fluctuations were driven by internal processes.

[18] With the solar wind density increase at 1500, Earth's magnetopause was pushed in and Geotail moved into the magnetosheath; before the data gap Geotail was in the magnetosphere (not shown). Geotail fluctuations (top three panels) have a strong compressional component possibly corresponding to the increased solar wind fluctuations but are dominated by b_y (torodial) fluctuations. Because of the data gap at Geotail and because the magnetosheath (shaded region) is turbulent, it cannot be certainly established that fluctuations turn on in the same way as at GOES. At 2300 on 20 March, Geotail crossed the Sun-Earth line at the nose of the magnetopause and shortly after passes back into the magnetosphere. The b_y fluctuations were greatly reduced in the magnetosphere. Enhanced fluctuations occurred again at Geotail about 0200 on 21 March and increased with movement along the dusk flank.

[19] Cluster observations are available starting at about 1930 on 20 March (bottom three panels in Figure 3). We show Cluster 1 observations; the satellites are close together at this time (~100 km) and show similar features. At about 2000 Cluster-1 crossed the ecliptic plane with its orbit taking it over the northern polar region starting about 0015 on 21 March, including the plasma mantle and cusp, then into the magnetosheath about 0215 and out into the

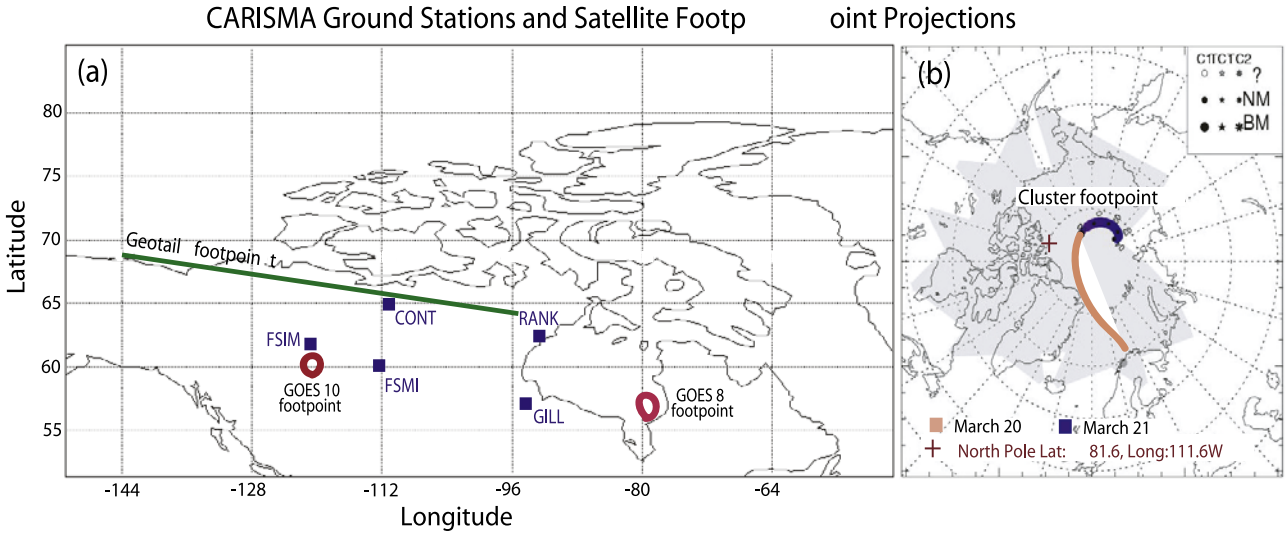

Figure 4. (left) Footpoints of the Geotail, Cluster, GOES 8 and GOES 10 satellites for data interval a in the northern hemisphere and (right) footpoints of Cluster over the norther polar region.

solar wind just after 0600 (see also *Lavraud et al.* [2004]). When Cluster was in the cusp from about 0015 to 0200, identified by a typical decrease in magnetic field magnitude (not shown), the compressional (b_z) component was dominant as seen in Figure 3. With entry into the magnetosheath, transverse fluctuations increased dramatically both in the radial (b_x) and azimuthal (b_y) components. The footpoint plot shows Cluster to be on dayside closed field lines (Figure 4), but this is not born out in either the Cluster CIS HIA (ion) observations (not shown) or FGM magnetic field observations compared against solar wind values. In the solar wind the fluctuations dropped to a low level.

[20] We show in Figure 4 satellite footpoints for Geotail, Cluster, GOES 8 and GOES 10 near CARISMA ground stations in the northern hemisphere for interval a using SSCWeb (left) and Cluster footpoints over the north pole using the Leicester plots (right). RANK and CONT are at the footpoints of field lines near the magnetopause, GILL is at a footpoint of field lines near GOES 8, and FSIM and FSMI are at the footpoints of field lines near GOES 10. The initial time span at the onset of the ICME (20 March 1000–1600) had the best correlations between compressional power in the solar wind, magnetosphere and ground observations. Between ACE or Wind and geostationary satellites, the correlation is between 0.52 and 0.67. Between ACE or Wind and ground stations the correlations are reduced to between 0.34 and 0.56 for this initial period. However, between geostationary satellites and ground stations near their footpoint, the correlation is ~0.8, indicating a strong linkage.

[21] We show power spectral densities (psd) during interval a in Figure 5. PSDs associated with the compressional fluctuations are seen at ACE and Wind in the solar wind, Geotail near the magnetopause, GOES 8 and 10 at geostationary orbit, and at Cluster over the northern pole. PSDs associated with horizontal (H) fluctuations are shown for five ground stations: RANK, CONT, GILL, FSIM, and FSMI. Because the ground-based fluctuations are modulated by the ionosphere we concentrate on the power and not the wave form in the comparisons with solar wind and magnetospheric fluctuations. There were powerful pressure fluctuations at the leading edge of the high-speed stream ~1500–1800 on 20 March observed at all locations with the exception of Cluster where no data is available. There was broadband input from the solar wind in the Pc5 frequency range, with the strongest power concentrated in the range from 0.5 to 4 mHz (especially visible at ACE in the top panel). On the ground at footpoints connected to the magnetopause (RANK, CONT), power peaks were concentrated under 2 mHz with a couple of exceptions between 2 and 4 mHz. At ground stations near footpoints of GOES satellites power peaks were patchy through the 1–4 mHz range. The patchy pattern was similar at the GOES satellites but the power at GOES was reduced by at least a factor of 10. The power at the ground based stations was larger than the solar wind input and was concentrated at frequencies less than 2 mHz for RANK and CONT. This suggests a global mode resonance may be excited at the magnetopause; the frequency range corresponds to the lowest cavity eigenfrequencies. The strongest power lasted only these few hours but some enhanced power continued through 20 April.

3.2. Interval b

[22] The top two panels of Figure 6 show ACE and Wind data for interval b, 25–26 March, with ACE (blue) and Wind (black) data. ACE remains 225 R_E upstream near the Sun-Earth line; Wind is 80 R_E upstream but only 30–50 R_E off the Sun-Earth line on the dusk side. This interval contains a density (top panel) and pressure fluctuation (second panel) increase from about 1430 on 25 March to 0300 on 26 March. The speed remains nominal during this interval but afterward at 1100 on 26 March increases to 600 km/s. The magnetospheric response directly attributable to the solar wind, however, occurs during the interval shown. During this interval the IMF is northward until about 2100 on 25 March, when it begins oscillating between northward and southward. ACE and Wind parameters track

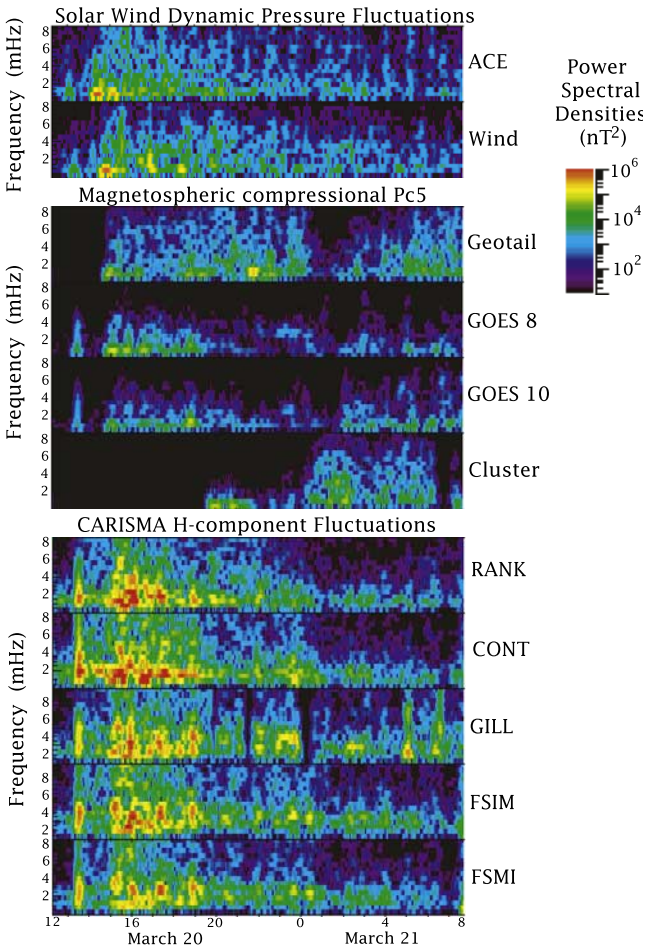

Figure 5. Power Spectral Densities at ACE, Wind, Geotail, GOES 8 and 10, Cluster, and CARISMA ground stations near the satellite footpoints.

together well; ACE pressure fluctuations are not shown in the second panel for clarity.

[23] The bottom nine panels of Figure 6 show wave forms for magnetospheric fluctuations for the Geotail and GOES 8 and 10 satellites. When the density and pressure fluctuations decreased at 0300, Geotail moves back into the magnetosphere (magnetosheath is shaded) as seen in the third through the fifth panels. A dotted line through the b_x, b_y, and b_z components for each satellite indicates the time the satellite crossed the Sun-Earth line, i.e., its position is near the subsolar point. A solid vertical line is also shown that corresponds to the increase in solar wind pressure fluctuations. Increased compressional fluctuations are seen at the two GOES satellites at the solid line; a larger compressional component compared to the other components. The fluctuations are stronger at GOES 8 on the day side than at GOES 10 on the dawn flank at the time of the solid vertical line. Six hours later the compressional fluctuations are stronger at GOES 10 now on the dayside than at GOES 8 now on the dusk flank. This effect is also seen at Geotail, but the subsolar magnetopause is quiet. During the time when Geotail was at the subsolar point, the solar wind fluctuations were smaller than on either side. The increased fluctuations at GOES are as large as in interval a in spite of the nominal solar wind speed. From this example we can say that increases in solar wind pressure fluctuations are more directly controlling magnetospheric compressional Pc5.

3.3. Interval c

[24] Solar wind parameters for 5–6 April 2002, interval c, are nominal. ACE is 225 R_E upstream near the Sun-Earth line, and Wind 50 R_E upstream but off the Sun-Earth line 100 R_E on the duskside. V_{sw} is between 350 and 450 km/s, N is between 2 and 7/cc. The IMF is oscillating between northward and southward, between −5 and 10 nT. The pressure fluctuations are smaller than those seen in intervals a and b, ±5 nPa. Compressional fluctuations (b_z component) were still dominant on the dayside at Geotail and GOES but were much smaller than the fluctuations in intervals a and b. The amplitude of the compressional fluctuations at Geotail were larger off the Sun-Earth line on the dayside. For GOES 8 and 10, the fluctuations died away on the flanks and the toroidal (b_y) component remained small. Between 0400 and 1200 on 6 April Geotail passed back and forth between the magnetosphere and magnetosheath several times. Fluctuations in all components were larger in the magnetosheath and b_y was significant. For the rest of the interval Geotail was just inside the magnetopause; the compressional (b_z) fluctuations remained the largest component on the dayside, but the toroidal (b_y) component became of comparable size on the flanks.

[25] We show the power spectral densities associated with the compressional fluctuations for satellites and horizontal (H) fluctuations for ground stations in Figure 7. The format is the same as in Figure 5. As with interval a the power on the ground is greater than that at magnetospheric satellites. This is a quiet day, with no strongly driven times as was evident in intervals a and b. There are, however, solar wind bursty broadband peaks in the dynamic pressure fluctuations throughout the interval, many of which are reflected in the magnetospheric and ground data. For example, initially in Figure 7, ACE and Wind show broadband power in the Pc5 frequency range from about 1000 to 1500 on 5 April. Enhanced power at the lower half of the Pc5 range is seen at RANK and CONT (at footpoints attached to the magnetopause) and to a lesser degree at GILL, FSIM and FSMI (at footpoints connected to geostationary orbit). RANK is on the dayside from about 1400–2000 and CONT from about 1700–2300, so these strong enhancements are on the dawn and dayside regions. Geotail, GOES 8 and 10 show corresponding enhanced power for these intervals but the enhancement is significantly less than that seen in the solar wind or on the ground. The power at the dayside magnetopause (RANK, CONT, DAWS, Geotail) is greater than that at dayside geostationary orbit (GILL, FISM, FSIM, GOES8, and 10).

[26] Correlations between GOES 8 and GILL and between GOES 10 and FSIM and FSMI remain good during this not strongly driven interval, about 0.7 in each case on April 5. Geotail is not fixed above a ground station, and thus is not as well correlated with any ground station except during short intervals. The correlations between solar wind satellites and magnetospheric satellites or ground based stations are poor except during the intervals discussed

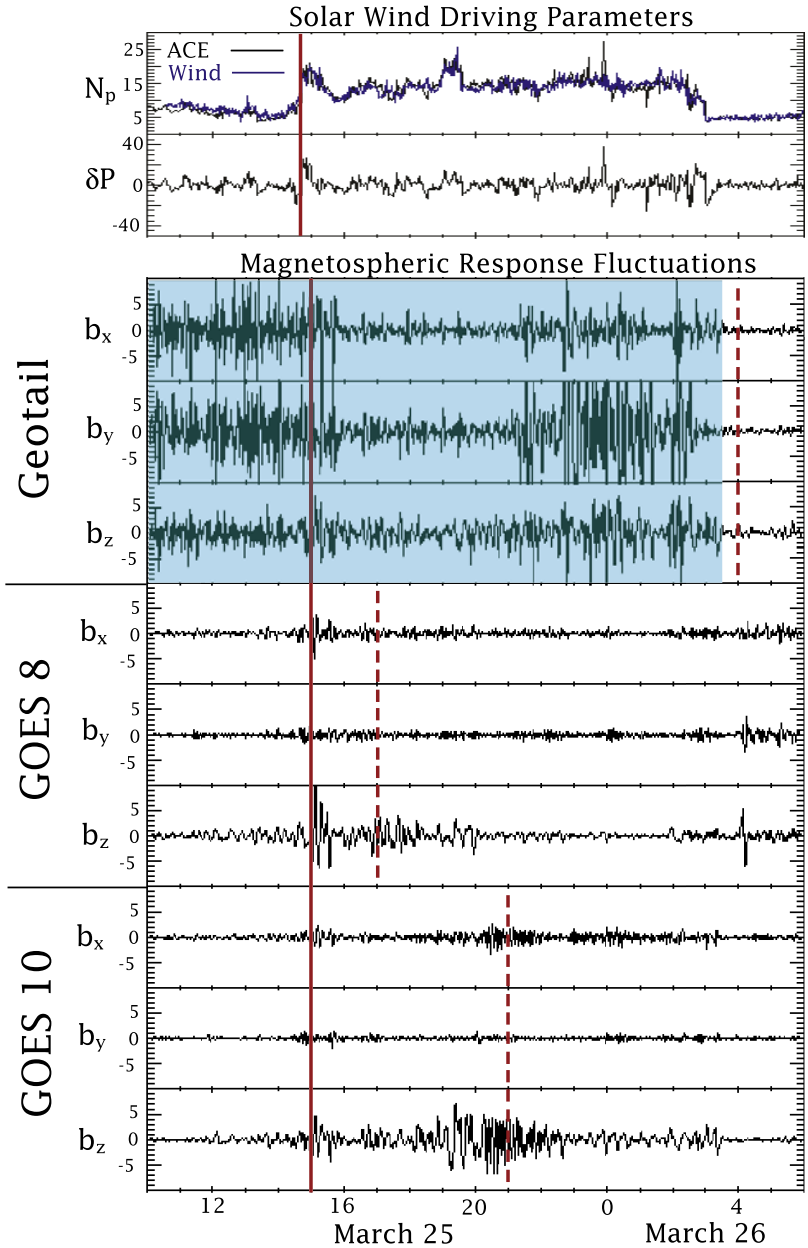

Figure 6. Fluctuations in magnetic field for the Geotail, GOES 8 and 10, and Cluster satellites during interval b.

above, i.e., 5 April 1000–1500, 1700–1900; 6 April 0700, 1000–1400, when the correlations are generally 0.5 or greater. The magnetopause observations (Geotail) are well correlated with solar wind bursts. GOES 8 and 10 have fewer peaks, but these are well correlated with solar wind bursts.

3.4. Poynting Flux

[27] Fluctuations in the solar wind dynamic pressure perturb the magnetopause and transmit fast-mode magnetosonic waves and shear-Alfvén waves into the inner magnetosphere. These waves propagate in the direction of the Poynting Flux, S. We examine the Poynting Flux at the magnetopause using Geotail data for events in section 3. We determined the Poynting Flux due to compressional fluctuations near the magnetopause, defined as

$$\mathbf{S} = \mathbf{e} \times \mathbf{b_c} \tag{1}$$

where $\mathbf{e}$ are the electric field fluctuations and $\mathbf{b_c}$ are the compressional fluctuations discussed in section 3. Electric field fluctuations are determined by subtracting the background (smoothed) field, $\mathbf{E_0}$ from the 2-D electric field from the Geotail EFD instrument.

$$\mathbf{e} = \mathbf{E} - \mathbf{E_0} \tag{2}$$

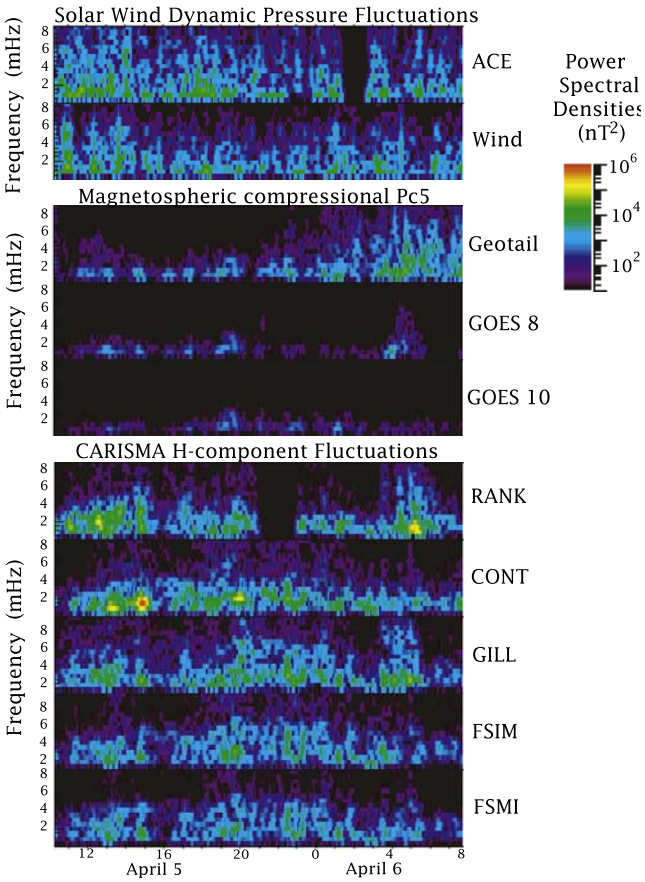

Figure 7. Power Spectral Densities at Wind, Geotail, GOES 8 and 10, Cluster, and CARISMA ground stations near the satellite footpoints.

Just inside the dayside magnetopause near the ecliptic plane the direction of the background magnetic field, Earth's dipole field, is primarily in the z GSE direction. Compressional fluctuations are in the direction of the background magnetic field, approximately in the z GSE direction in this limited region. We previously showed wave forms near the dayside magnetopause with Geotail data to be strongest in the compressional component. For this discussion, we separated these compressional fluctuations out and ignored the transverse wave components that are less significant. The Electric Field data from the Geotail EFD instrument is only available in the GSE x-y plane. However, $\mathbf{e_x}$ and $\mathbf{e_y}$ are sufficient inside just inside the dayside magnetopause to determine the Poynting Flux for compressional fluctuations since the cross product of $\mathbf{e_z}$ and b_c is approximately zero. In the following examples, we show only the time ranges in which these approximations to the Poynting Flux are valid.

[28] In Figure 8 we show the direction of the Poynting Flux, **S**, along the orbit of Geotail (in GSE coordinates) for interval c using the VisBARD visualization tool. We are looking down on the x-y GSE plane that shows the significant components (S_z is about 13% of the overall Poynting Flux in this interval). We begin with the interval of nominal solar wind to examine the nearly static magnetopause. During interval c, Geotail is skimming along inside the magnetopause from 5 April 0600 to 6 April 0800 in 2002. Geotail crossed the subsolar point at 1750 on 5 April. Along Geotail's orbit, **S** is oscillating primarily inward and outward with a net inward flux. Approximately 2/3 of the flux is directed inward and 1/3 outward so that overall there is a net inward flux of about 1/3. Near the magnetopause nose **S** is less ordered, still oscillating but some flux is directed away from the surface normal, along the surface itself. The disorder increases on the duskside.

3.5. Statistics

[29] We examined the entire interval from 20 March 2002 to 2 May 2002 to elucidate the solar wind excitation of Pc5 fluctuations within the magnetosphere. Solar wind conditions varied during the interval with both northward and southward IMF, with periods of high and low pressure, and with speeds from 300 km/s to nearly 800 km/s, ICMEs and HSSs occurred copiously. In the following we fold the ICMEs, HSSs, and nominal intervals together and examine them statistically. We first examine solar wind dependencies by local time, and then examine power dependency on specific solar wind parameters.

[30] Figure 9 shows the solar wind total power plotted against the total power at GOES 8/10 (top panel), at ground stations near magnetopause footpoints (middle panel), and at ground stations near GOES 8/10 footpoints (bottom

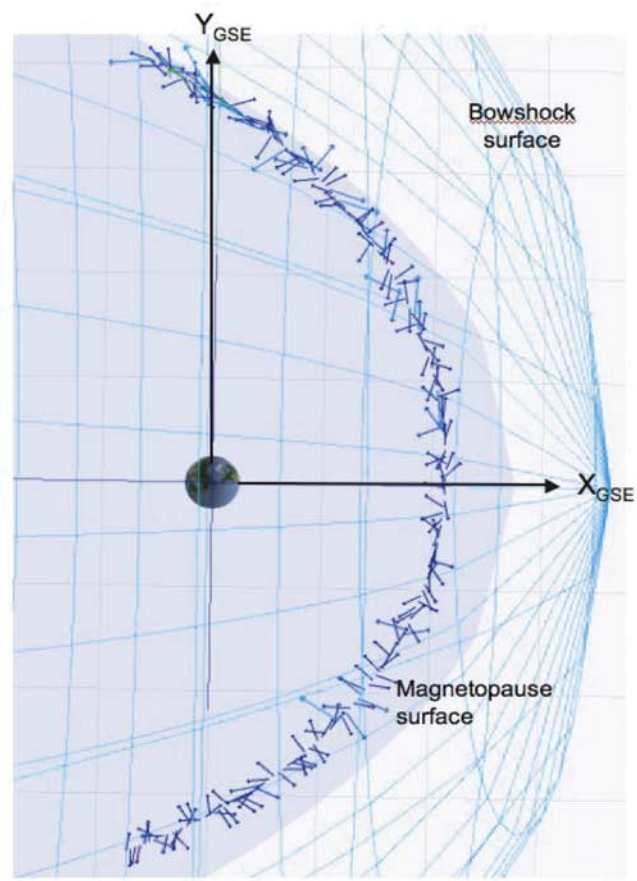

Figure 8. Interval b: Poynting Flux at the Geotail satellite inside the magnetosphere from 5 April 0600 to 6 April 0800 in 2002. Geotail crossed the subsolar point at 1750 on 10 April.

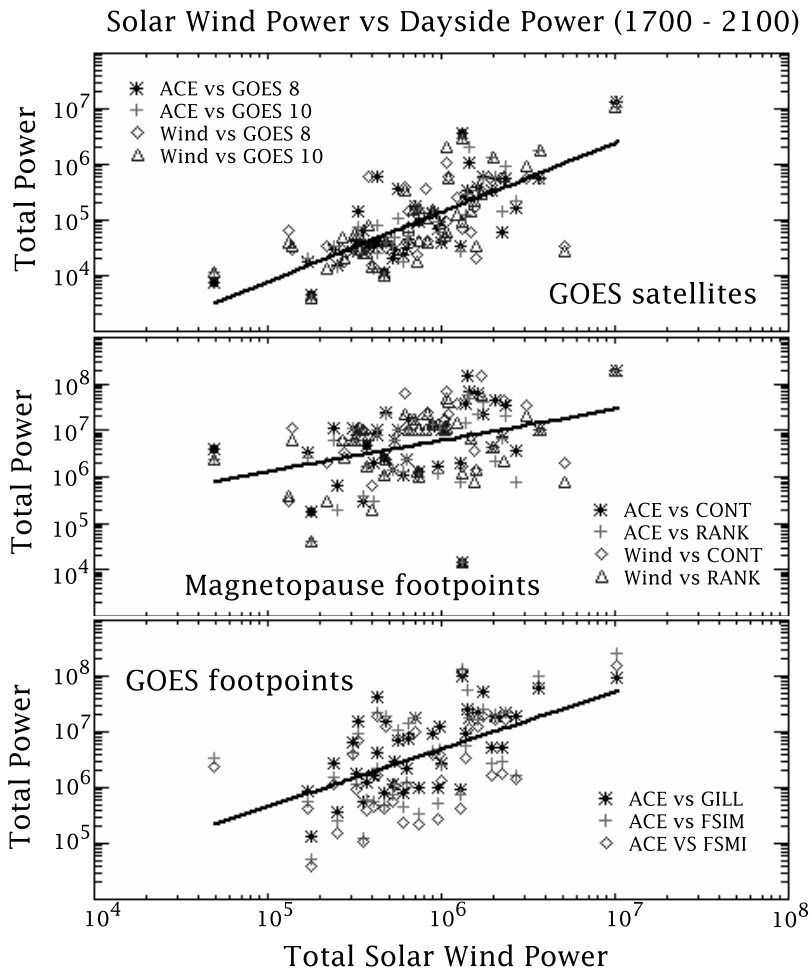

Figure 9. During intervals when magnetospheric satellites are on the dayside: (top) total power in the solar wind versus total power at GOES 8/10 versus (middle) total power on the ground near footpoints connected to the magnetopause and versus (bottom) total power on the ground near footpoints connected to GOES 8/10.

panel) for dayside intervals from 20 March 2002 to 2 May 2002. Each symbol on these plots corresponds to the dayside portion of a single day. ACE and Wind are each plotted against the magnetospheric monitors in the top and middle panels, but in the bottom panel only ACE is plotted against GILL, FSIM, and FSMI. In each panel we also show a linear least squares fit (LSF) to the data. Taking the LSF values to be the running mean, we also determine the average variance from the mean. The slope of the LSF in the top panel on a log-log scale is 0.83 ± 0.09. The average variance on the same scale is 0.36. Thus there is a strong dependence for GOES 8/10 total power to increase with an increase in solar wind power (top panel). At magnetopause footpoints the slope decreases to 0.42 ± 0.13, and the average variance increases to 0.57. The dependence for ground stations near GOES 8 and 10 footpoints (bottom panel) is weaker than at GOES in space, 0.65 ± 0.11 and has a larger variance, 0.53. The ground stations have additional sources causing power fluctuations; the dependence on solar wind power is more tenuous. Ground station magnetometers are sensing magnetospheric fluctuations that are modulated through the ionosphere. In addition, ground magnetometers also respond to telluric currents as discussed, for example, by *Pilipenko and Fedorov* [1994]. If the telluric currents could be separated from the magnetospheric/ionospheric currents, then the latter would likely be more closely tied to the corresponding satellite data.

[31] Table 1 shows the linear least squares fit slopes and average variances for all four local time sectors: day, dawn, dusk, and night. What stands out most from this table is that there is not a lot of variation with local time except that the variances are higher on the night side and at the footpoints. The ground stations near magnetopause footpoints show the least difference with local time; GOES satellites and footpoints show more difference. On the dawn flank, the GOES LSF slope is softer than on the dayside, 0.80 ± 0.08, while on the dusk side the LSF slope is harder, 0.94 ± 0.08 The dusk and nightside slopes include internally generated fluctuations that occur in response to southward IMF. The increase is measurable but not larger than the direct response. At geostationary footpoints the LSF slope is harder on the dawnside than on the dayside, 0.85 ± 0.13, and is even harder than in space, but has a much larger average variance, 0.67. On the duskside near geostationary footpoints the LSF slope is 0.77 ± 0.09. On the nightside the slopes of the LSF for the three plots are 0.90 ± 0.12, 0.40 ±

Table 1. Total Power in Solar Wind Versus Total Power in Magnetosphere[a]

	GOES		Magnetopause Footpoint		GOES Footpoint	
	Slope	Variance	Slope	Variance	Slope	Variance
Day	0.82 ± 0.09	0.36	0.42 ± 0.13	0.57	0.65 ± 0.11	0.53
Dawn	0.80 ± 0.08	0.38	0.43 ± 0.11	0.49	0.85 ± 0.13	0.67
Dusk	0.94 ± 0.08	0.40	0.45 ± 0.07	0.33	0.77 ± 0.09	0.49
Night	0.90 ± 0.12	0.60	0.40 ± 0.15	0.77	0.82 ± 0.15	0.75

[a]Linear least squares fit slopes of total power in the solar wind versus total power in the magnetopshere at three locations: GOES and ground stations near magnetopause and GOES footpoints.

0.15, and 0.82 ± 0.15, from top to bottom. The average variances are larger than at other local times, 0.60, 0.77, and 0.75 from top to bottom. Together these statistics show that compressional magnetospheric power has a strong dependency on solar wind power throughout magnetospheric local time across a broad range of solar wind parameters. The solar wind pressure fluctuations excite a nearly global response.

[32] Next we discuss statistical dependence on specific solar wind parameters in different geospace regions. Figure 10 shows total power during the interval 20 March 2002 to 2 May 2002 in the solar wind versus solar wind density (top panel), solar wind speed (second panel), solar wind dynamic pressure (third panel), and IMF B_z (fourth panel); each symbol on these plots corresponds to total power in a four hour segment during the interval. For comparison purposes it makes most sense to discuss the order of magnitude change in power across the range of each solar wind parameter rather then the slope of the change. Otherwise we would get a false high slope ($m = \Delta y/\Delta x$) comparing the power change with Pressure (Δx = 12 nPa) to the power change with solar wind speed (Δx = 500 km/s).

[33] In Figure 10 the solar wind power at ACE and Wind increases most strongly with dynamic pressure (third panel), ~3.5 orders of magnitude across the full range of P. After that, the solar wind power increases most with N_p (2.5 orders of magnitude), then V_{sw} (1.1 orders of magnitude), and finally B_z (<1 order of magnitude). The average variances increase in this same order, i.e., 0.36, 0.48, 0.52, and 0.56, for P, N_p, V_{sw}, and B_z, respectively. Table 1 lists all of the order of magnitude changes and the average variances for the solar wind, and also at GOES, at magnetopause footpoints and at GOES footpoints. At GOES the dependencies are similar to those in the solar wind with one exception: GOES power increases almost twice as much with solar wind speed compared to the power at ACE and Wind. The average variances in all cases are higher at GOES than in the solar wind.

[34] The total power at ground stations near footpoints connected to the magnetopause and and near footpoints connected to the GOES 8 and GOES 10 satellites, both show the doubling in power with solar wind speed seen at the GOES satellite and compared against the power in the solar wind. On the ground the dependence on solar wind density is gone, both cases are relatively flat across the range of N_p. This lowers the dependence on P also. The dependence on B_z at the magnetopause footpoint is about the same as in the solar wind and at GOES, but at GOES footpoints the increase in total power doubles with B_z. The

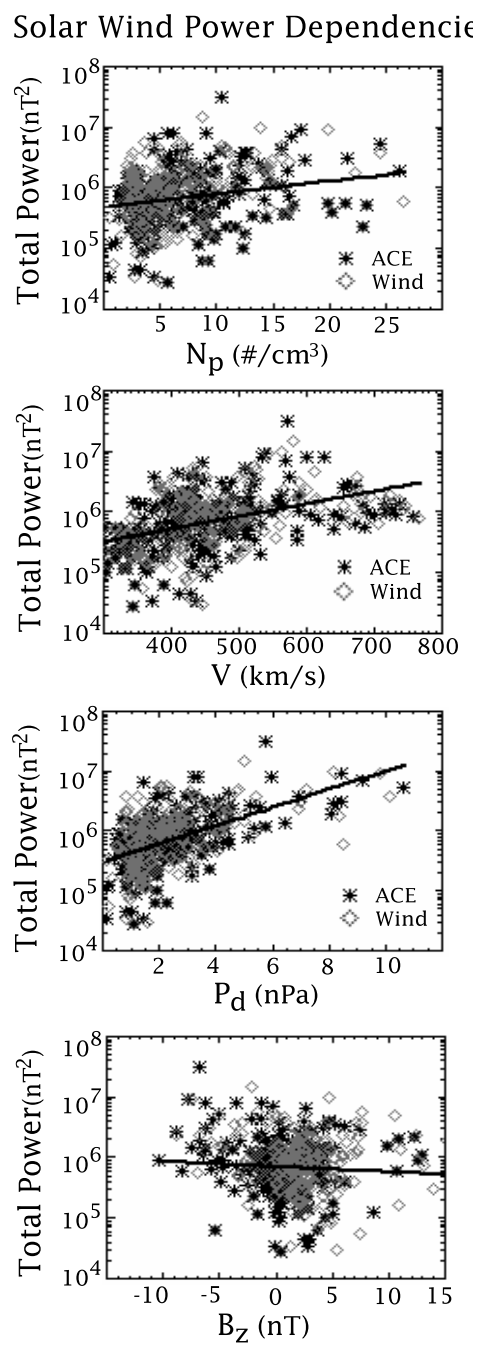

Figure 10. Total power in the solar wind with linear least squares fit for four solar wind parameters in the panels from top to bottom.

most important difference between the signal and response is that the response is stronger for higher solar wind speeds.

4. Discussion

[35] The observations presented in the previous section can be grouped into two major categories: (1) observations showing either external or internal forcing and (2) observations showing an external excitation process at play. We discuss the implications in this section, whether the observations confirm, contradict, or complement previous observations and how our understanding of Pc5 is affected.

[36] Some previous studies of compressional Pc5 have included analysis of solar wind pressure fluctuations driving magnetospheric waves. *Zhu and Kivelson* [1991] found compressional Pc5 waves on the dayside that they attributed to solar wind dynamic pressure variations. *Kepko et al.* [2002] showed pressure fluctuations at the same discrete frequencies in the solar wind as compressional waves at geostationary orbit. The results presented here confirm and extend their conclusions. This study underlines the importance of solar wind excitation as an important source of compressional Pc5 fluctuations, especially during the declining phase of the solar cycle with numerous HSSs. *Zhu and Kivelson* [1991] had incomplete coverage of the dayside and so could not comment on its importance. *Kepko et al.* [2002] showed an event study. *Kessel et al.* [2003] showed sustained geomagnetic pulsations in the noon and midnight sectors during times of sustained dynamic pressure fluctuations in the solar wind. They set the stage for the current study.

[37] During our interval, solar wind pressure fluctuations in the Pc5 range were nearly ubiquitous and excited compressional Pc5 fluctuations in the magnetosphere. The amplitude and power of the excited fluctuations were in direct proportion to the input amplitude and power as shown, for example, in Figure 9 and Table 1. The amplitude and power were largest near the leading edge of HSSs and ICMEs, as in interval a (20 March at about 1430 in Figures 2, 3, and 5). *Kessel et al.* [2003] also focused on the declining phase of the solar cycle (previous cycle), but *Zhu and Kivelson* [1991] excluded times of large solar wind events. Quiet solar wind conditions exhibited small pressure fluctuations and these could be seen in the magnetosphere and on the ground. For example, interval c contained solar wind bursty broad band peaks in the dynamic pressure fluctuations throughout the interval, many of which were reflected in the magnetospheric and ground data (from about 1000 to 1500 on 5 April in Figure 7). The magnetospheric and ground response in these cases was weak because the solar wind driving fluctuations were likewise weak.

[38] *Anderson*'s [1994] review of ULF pulsations found that the primary occurrence region of compressional Pc5 was on the dusk flank at large L (his Figure 1). *Zhu and Kivelson* [1991] using ISEE-1/2 found that compressional Pc5 waves were a common feature near the two flanks of the magnetosphere. The observations presented here complement these results in that non-solar-wind-driven fluctuations were observed primarily on the nightside flanks, especially the dusk flank as seen, for example, at GOES 10 starting about 0200 on April 21 (Figure 3). Table 1 shows that the power is slightly higher at GOES at dusk and night, though at GOES footpoints the power is higher also at dawn. The IMF was southward during portions of these intervals so the increases were likely due to internal magnetospheric processes as discussed by *Barfield and McPherron* [1972] and *Anderson* [1994]. However, the increases at GOES on the dusk flank and nightside are only 14–17% greater than the dayside and dawnside. This finding shows that for this interval the power due to external forcing is greater than that due to internal forcing, which contradicts the conclusion of *Anderson* [1994] as to the primary occurrence region. This study finds the response to be essentially global though strongest on the dayside. Because this study focused on a time period during the declining phase of the solar cycle with numerous HSSs, the results may be biased toward solar wind driven effects that are not as significant during other intervals.

[39] It is worth noting that the declining phase of the solar cycle is a time of high magnetospheric activity. *Li et al.* [2003] claimed that the declining phase of the solar cycle is the most geoeffective phase. They equated geoeffectiveness to strong increases in two parameters: outer radiation belt flux or so-called "killer" electrons (SAMPEX 2–6 MeV electrons) and the D_{st} index of the strength of magnetic storms. Their Figure 1 illustrates the strength of their claim for the last solar cycle with the strongest negative D_{st} and electron fluxes occurring during the declining phase. The declining phase of the solar cycle is characterized by long-lasting recurrent HSSs, many leading to strong magnetic storms. Adding to that, many studies have shown a linkage between HSSs, "killer" electrons, and ULF waves [e.g., *Rostoker et al.*, 1998; *Baker et al.*, 1998; *Mathie and Mann*, 2000]. If solar wind forcing is dominant during this phase as we have shown, then it is important to factor this into our understanding of the overall picture.

[40] Geotail observed compressional Pc5 fluctuations just inside the magnetopause. These fluctuations had more power than compressional fluctuations at dayside geostationary orbits. These observations suggest that power was dissipating on the inward journey and is in agreement with *Zhu and Kivelson* [1991] who found that waves were largest at the magnetopause, decreasing in power with lower L shell. This effect can be seen with Geotail, GOES 8 and GOES 10 data in interval c from 1500 to 2000 on 5 April (Figure 7), and with ground-based stations from 1500 to 2000 in interval a on 20 March (Figure 5). In the latter case RANK and CONT were near footpoints connected to the magnetopause, while GILL, FSIM, and FSMI were near footpoints connected to geostationary orbit. The direction of the Poynting Flux along the orbit of Geotail, that is, along the magnetopause, is inward as can be seen in Figure 8. The Poynting flux due to the compressional fluctuations was highly oscillatory inward and outward along the orbit of Geotail with a small net inward flux. These observations do not unambiguously pinpoint the transmission mechanism but do suggest that fluctuations are excited near the magnetopause and propagate evanescently into the magnetosphere on the dayside.

[41] Ground observations at CARISMA ground stations RANK and CONT (near magnetopause footpoints) were strong during intervals a and b as seen in Figures 3 and 6. RANK and CONT were near footpoints connected to the

Table 2. Total Power Dependencies on Solar Wind Parameters[a]

	Solar Wind		GOES		Magnetopause Footpoint		GOES Footpoint	
	Δ T P	Variance	Δ T P	Variance	Δ T P	Variance	Δ T P	Variance
N_p	2.5	0.48	1.9	0.68	−0.01	0.65	0.6	0.76
V_{sw}	1.1	0.52	2.0	0.61	2.0	0.55	2.1	0.59
P	3.5	0.36	3.0	0.56	1.3	0.63	2.7	0.68
B_z	−0.9	0.56	−1.1	0.70	−0.9	0.64	−2.0	0.72

[a]Order of magnitude change of total power (Δ T P) versus solar wind parameter in the solar wind, at GOES, and at ground stations near magnetopause and GOES footpoints.

dayside magnetopause between about 1500–2400 each day. Geotail's orbit and solar wind conditions occasionally allowed a comparison. On 5 April a correlation analysis was possible with Geotail, RANK, and CONT data between 1500 and 2400; the correlation varied between 0.7 and 0.9. RANK and CONT ground stations can serve as a proxy to the magnetopause when Geotail data is not available, though because the magnetopause moves inward and outward with changing solar wind conditions, the proxy relationship may not always be accurate.

[42] CARISMA ground station GILL is near the footpoint of GOES 8, while FSIM and FSMI are near the footpoint of GOES 10. For interval a there was a strong correlation (0.8) between GOES 8/10 and their corresponding ground stations. The footpoint relationship with the geostationary GOES satellites is more stable than with those near the magnetopause. Other intervals also had good correlation. For example, interval c was a quiet day, with no strongly driven times as was evident in interval a. There were, however, correlations between GOES 8 and GILL, and between GOES 10 and FSIM and FSMI that remained good during this not strongly driven interval, about 0.7 in each case on 5 April.

[43] The good correlation between satellites and ground stations near their footpoints, along with oscillating Poynting Flux in the y and z directions support the likelihood of a field line resonance (FLR) having been excited. *Kivelson and Southwood* [1991], and more recently, *Rae et al.* [2005] discussed a FLR excited at the magnetopause that that traveled into the ionosphere and then to the ground. Our observations confirm these results at the magnetopause. In the ionospheric transitor model [*Engebretson et al.*, 1991] it would seem probable that power input would elucidate a global response, or at least similar power at L shells. There is some evidence for this in similarities at the two GOES satellites. However, in the examples, dayside compressional fluctuations were stronger than dawn or dusk compressional fluctuations. Additionally, compressional fluctuations first observed at Geotail were later observed at GOES satellites with less power. We also note that the ground stations had much higher power than their corresponding satellites. This is likely due to the ground stations being at the antinode of the standing oscillation and the satellites being at the node [e.g., *Hughes*, 1994].

[44] Solar wind driven compressional fluctuations were the dominant component on the dayside, just inside the magnetopause and at geostationary orbit. For example in interval a (1500–2000 on 20 March in Figure 3), the strongest component in the GOES data was the compressional (b_z) component. Just inside the magnetopause compressional fluctuations were the largest component on the dayside, but the toroidal component became of comparable size on the flanks. This can be seen with Geotail data in Figure 3. *Anderson* [1994] showed toroidal Pc5 waves to be mainly on the dawn flank, stronger at higher L shells. Our results confirm the existence of toroidal Pc5 waves on the flanks inside the magnetopause. The most frequently cited source of these flank Pc5 pulsations is the Kelvin-Helmholtz (K-H) instability at the magnetopause [e.g., *Dungey*, 1955; *Miura*, 1992; *Anderson*, 1994]. Fast magnetosheath flow excites surface waves on the magnetopause that become Kelvin-Helmholtz unstable [e.g., *Miura*, 1984]. Our Table 2 shows that magnetospheric power increases with solar wind speed. *Mann et al.* [1999] have recently shown that for very large flow speeds at the magnetopause flanks, the K-H instability can energize body type waveguide modes. *Samson et al.* [1992] showed that discrete frequencies at approximately 1.3, 1.9, 2.6, and 3.4 mHz were compatible with MHD waveguide and cavity modes in the magnetosphere. The driving and response frequencies in this study are primarily in the range 0.5–4 mHz. All of this evidence along with the essentially global response seen in Table 1 suggests global mode excitation was in existence.

5. Conclusions

[45] In March and April 2002, there was a favorable alignment of satellites that facilitated a study of transient fluctuations in the Pc5 frequency range. There were approximately 10 large events in this interval (ICMEs and HSSs); we examined them all and selected two as representative. We also detailed an interval of nominal solar wind for comparison. We can group our findings into two major bullets: (1) the importance of external versus internal forcing and (2) multiple external excitation processes at play.

[46] First, for this interval in the declining phase of the solar cycle with multiple HSSs and ICMEs, external forcing due to solar wind dynamic pressure fluctuations was dominant over internal forcing. We found the following specific indicators:

[47] 1. Dynamic pressure fluctuations (Pc5 frequency range) were nearly ubiquitous in the solar wind, and they excited a response within the magnetosphere and on the ground, across a broad range of solar wind speed and dynamic pressure, and IMF B_z.

[48] 2. The amplitude and power of Pc5 compressional fluctuations in the magnetosphere, and on the ground near magnetopause or geostationary footpoints, were in direct proportion to the amplitude and power of Pc5 range fluctuations in the solar wind (Figure 9 and Table 1).

[49] 3. Fluctuations driven by internal processes, occurring primarily at dusk and on the nightside, accounted for less than 20% of the total power (Table 1).

[50] Second, multiple external forcing processes were occurring during this interval. Which of these processes is dominant remains unresolved. We found the following evidence:

[51] 1. Evanescent propagation, in which solar wind driven waves were observed throughout the magnetosphere but were strongest in the dayside magnetosphere. Compressional fluctuations just inside the dayside magnetopause had more power than compressional fluctuations at dayside geostationary orbits. These observations together with the existence of a net inward Poynting flux from the magnetopause suggest evanescent propagation of compressional fluctuations inward from the magnetopause.

[52] 2. FLR, in which Poynting flux due to the compressional fluctuations was oscillatory in all components, including along field lines. Dayside satellite power correlated well with power at ground based stations near their magnetic footpoint for strongly driven solar wind fluctuations. These observations support a field line resonance (FLR) having been excited at the magnetopause that traveled into the ionosphere and to the ground.

[53] 3. Global modes, in which the driving and response frequencies primarily were in the range 0.5 to 4 mHz, corresponding to cavity and waveguide eigenfrequencies. The total power in the magnetosphere increased with solar wind speed, and toroidal fluctuations were dominant on the magnetopause flanks. These observations support a K-H instability energizing body type waveguide modes.

[54] **Acknowledgments.** We obtained most of the data for this study from CDAWeb (cdaweb.gsfc.nasa.gov) and also used the SSCWeb (sscweb.gsfc.nasa.gov) interface for orbits and footpoints. We also thank the instrument PIs for supplying data to CDAWeb. Cluster footpoint plots were obtained from the University of Leicester (http://ion.le.ac.uk/cluster/). The authors thank the CARISMA magnetometer team for the provision of CANOPUS magnetometer data. The operation of the CARISMA (formerly CANOPUS) magnetometer array is funded by the Canadian Space Agency.

[55] Zuyin Pu thanks the reviewers for their assistance in evaluating this paper.

References

Anderson, B. J. (1994), An overview of spacecraft observations of 10s to 600s period magnetic pulsations in the Earth's magnetosphere, in *Solar Wind Sources of Magnetospheric Ultra Low-Frequency Waves*, *Geophys. Monogr. Ser.*, vol. 81, edited by M. J. Engebretson, K. Takahashi, and M. Scholer, p. 25, AGU, Washington, D. C.

Baker, D. N., et al. (1998), Coronal mass ejections, magnetic clouds and relativistic magnetospheric electron events: ISTP, *J. Geophys. Res.*, *103*, 17,279.

Balogh, A., et al. (2001), The Cluster magnetic field investigation: Overview of in-flight performance and initial results, *Ann. Geophys.*, *19*, 1207.

Barfield, J. N., and R. L. McPherron (1972), Statistical characteristics of storm-associated Pc 5 micropulsations observed at synchronous equatorial orbit, *J. Geophys. Res.*, *77*, 4720.

Burlaga, L. F. (1968), Microscale structures in the interplanetary medium, *Sol. Phys.*, *4*, 67.

Chen, L., and A. Hasegawa (1974), A theory of long-period magnetic pulsation: 1. Steady state excitation of field line resonance, *J. Geophys. Res.*, *79*, 1024.

Dungey, J. W. (1954), Electrodynamics of the outer atmosphere, Rep. 69, Ions. Res. Lab., Pa. State Univ., University Park.

Dungey, J. W. (1955), Electrodynamics of the outer atmosphere, paper presented at Ionosphere Conference, Phys. Soc. of London.

Engebretson, M. J., L. J. Cahill Jr., R. L. Arnoldy, G. J. Anderson, T. J. Rosenberg, D. L. Carpenter, U. S. Inan, and R. H. Eather (1991), The role of the ionosphere in coupling upstream ULF wave power into the dayside magnetosphere, *J. Geophys. Res.*, *96*, 1527.

Engebretson, M. J., K.-H. Glassmeier, and M. Stellmacher (1998), The dependence of high-latitude Pc5 power on solar wind velocity and phase of high-speed solar wind streams, *J. Geophys. Res.*, *103*, 26,271.

Fairfield, D. H., et al. (1990), Upstream pressure variations associated with the bow shock and their effects on the magnetosphere, *J. Geophys. Res.*, *95*, 3773.

Fairfield, D. H., et al. (2003), Motion of the dusk flank boundary layer caused by solar wind pressure changes and the Kelvin-Helmholtz instability: 10–11 January 1997, *J. Geophys. Res.*, *108*(A12), 1460, doi:10.1029/2003JA010134.

Frank, L. A., K. L. Ackerson, J. A. Lee, M. R. English, and G. L. Pickett (1992), Comprehensive Plasma Instrument (CPI), Geotail Prelaunch Rep. 179, SES-TD-92-007SY, ISAS, location?.

Harrold, B. G., and J. C. Samson (1992), Standing ULF modes of the magnetosphere: A theory, *Geophys. Res. Lett.*, *19*, 811.

Hughes, W. J. (1994), Magnetospheric ULF waves: A tutorial with a historical perspective, in *Solar Wind Sources of Magnetospheric Ultra-Low-Frequency Waves*, Geophys. Monogr. Ser., vol. 81, edited by M. J. Engebretson, K. Takahashi, and M. Scholer, p. 265, AGU, Washington, D. C.

Kepko, L., H. E. Spence, and H. J. Singer (2002), ULF waves in the solar wind as direct drivers of magnetospheric pulsations, *Geophys. Res. Lett.*, *29*(8), 1197, doi:10.1029/2001GL014405.

Kessel, R. L., and S.-H. Chen, (1999), On the Earth's bow shock near solar minimum, in Interball in the ISTP Program: Studies of the Solar Wind-Magnetosphere-Ionosphere Interaction, NATO Sci. Ser., edited by D. G. Sibeck and K. Kudela, p. 87, Springer, New York.

Kessel, R. L., I. R. Mann, S. F. Fung, and D. Milling (2003), Correlation of Pc5 wave power inside and outside the magnetosphere during high speed streams, *Ann. Geophys.*, *21*, 1.

Kivelson, M. G., and D. J. Southwood (1991), Ionospheric traveling vortex generation by solar wind buffeting of the magnetosphere, *J. Geophys. Res.*, *96*, 1661.

Kivelson, M. G., J. Etcheto, and J. G. Trotignon (1984), Global compressional oscillations of the terrestrial magnetosphere: The evidence and a model, *J. Geophys. Res.*, *89*, 9851.

Kokubun, S., T. Yamamote, M. H. Acuna, K. Hayashi, K. Shiokawa, and H. Kawano (1994), The GEOTAIL magnetic field experiment, *J. Geomag. Geoelectr.*, *46*, 7–21.

Kwok, Y. C., and L. C. Lee (1984), Transmission of magnetohydrodynamic waves through the rotational discontinuity at the Earth's magnetopause, *J. Geophys. Res.*, *89*, 10,697.

Lavraud, B., et al. (2004),The exterior cusp and its boundary with the magnetosheath: Cluster multi-event analysis, *Ann. Geophys.*, *22*, 3039.

Lepping, R. P., and K. W. Behannon (1986), Magnetic field directional discontinuities: Characteristics between 0.46 and 1.0 AU, *J. Geophys. Res.*, *91*, 8725.

Lepping, R. P., et al. (1995), The Wind Magnetic Field Investigation, in *The Global Geospace Mission*, edited by C. T. Russell, pp. 207–229, Springer, New York.

Li, X., D. N. Baker, D. Larson, M. Temerin, G. Reeves, and S. G. Kanekal (2003), The predictability of the magnetosphere and space weather, *Eos Trans. AGU*, *84*(37), 361.

Mann, I. R., A. N. Wright, K. J. Mills, and V. M. Nakariakov (1999), Excitation of magnetospheric waveguide modes by magnetosheath flows, *J. Geophys. Res.*, *104*, 333.

Mathie, R. A., and I. R. Mann (2000), A correlation between extended intervals of ULF wave power and storm-time geosynchronous relativistic electron flux enhancements, *Geophys. Res. Lett.*, *27*, 3261.

Miura, A. (1984), Anomalous transport by magnetohydrodynamic Kelvin-Helmholtz instabilities in the solar wind magnetosphere interaction, *J. Geophys. Res.*, *89*, 801.

Miura, A. (1992), Kelvin-Helmholtz instability at the magnetospheric boundary: Dependence on the magnetosheath sonic Mach number, *J. Geophys. Res.*, *97*, 10,665.

Ogilvie, K. W., et al., (1995), SWE, Comprehensive Plasma Instrument for Wind Spacecraft, in Global Geospace Mission, edited by C. T. Russell, p. 55, Springer, New York.

Pilipenko, V. A., and E. N. Federov (1994), Magnetotelluric sounding of the crust and hydrodynamic monitoring of the magnetosphere with the use of ULF waves, in Solar Wind Sources of Magnetospheric Ultra Low-Frequency Waves, Geophys. Monogr. Ser., vol. 81, edited by M. J. Engebretson, K. Takahashi, and M. Scholer, p. 283, AGU, Washington, D. C.

Press, W. H., B. P. Flannery, S. A. Teukolsky, and W. T. Vetterling (1986), *Numerical Recipes, The Art of Scientific Computing*, Cambridge Univ. Press, Cambridge, U. K.

Rae, I. J., et al. (2005), Evolution and characteristics of global Pc5 ULF waves during a high solar wind speed interval, *J. Geophys. Res.*, *110*, A12211, doi:10.1029/2005JA011007.

Ramirez, R. W. (1985), *The FFT, Fundamentals and Concepts*, Prentice-Hall, Englewood Cliffs, N. J.

Rostoker, G., et al. (1998), On the origin of relativistic electrons in the magnetosphere associated with geomagnetic storms, *Geophys. Res. Lett.*, *25*, 3701.

Ruohoniemi, J. M., R. A. Greenwald, K. B. Baker, and J. C. Samson (1991), HF radar observations of Pc5 field line resonances in the midnight/early morning MLT sector, *J. Geophys. Res.*, *96*, 15,697.

Russell, C. T., and R. C. Elphic (1978), Initial ISEE magnetometer results: Magnetopause observations, *Space Sci. Rev.*, *22*, 681.

Samson, J. C., and R. Rankin (1994), The coupling of solar wind energy to MHD cavity modes, waveguide modes, and field line resonances in the Earth's magnetosphere, in Solar Wind Sources of Magnetospheric Ultra-Low-Frequency Waves, *Geophys. Monogr. Ser.*, vol. 81, edited by M. J. Engebretson, K. Takahashi, and M. Scholer, p. 253, AGU, Washington, D. C.

Samson, J. C., B. G. Harrold, J. M. Ruohoniemi, R. A. Greenwald, and A. D. M. Walker (1992), Field line resonances associated with MHD waveguides in the magnetosphere, *Geophys. Res. Lett.*, 19,441.

Sibeck, D. G., et al. (1989), The magnetospheric response to 8-minute period strong-amplitude upstream pressure variations, *J. Geophys. Res.*, *94*, 2505.

Singer, H. J., L. Matheson, R. Grubb, A. Newman, and S. D. Bouwer (1996), Monitoring space weather with GOES magnetometers, *SPIE Proc.*, *2812*.

Sonnerup, B. U. O., et al. (1981), Evidence of magnetic field reconnection the the Earth's magnetopause, *J. Geophys. Res.*, *86*, 10,049.

Southwood, D. J. (1974), Some features of field line resonances in the magnetosphere, *Planet. Space Sci.*, *22*, 483.

Wright, A. N., and G. J. Rickard (1995), A numerical study of resonant absorption in a magnetohydrodynamic cavity driven by a broadband spectrum, *Astrophys. J.*, *444*, 458.

Zhu, X., and M. G. Kivelson (1991), Compressional ULF waves in the outer magnetosphere, *J. Geophys. Res.*, *96*, 19,451.

Zurbuchen, T. H., and I. G. Richardson (2006), In-situ solar wind and magnetic field signatures of interplanetary coronal mass ejections, *Space Sci. Rev.*, *123*, 31–43.

R. L. Kessel, NASA Goddard Space Flight Center, Code 672, Greenbelt, MD 20771, USA. (mona.kessel@nasa.gov)